M. Marin, J. Citrin, L. Garzotti, M. Valovic, C. Bourdelle, Y. Camenen, F. J. Casson, A. Ho, F. Koechl, M. Maslov, JET contributors

Multipe-isotope pellet cycles captured by turbulent transport modelling in the JET tokamak

Multipe-isotope pellet cycles captured by turbulent transport modelling in the JET tokamak

M. Marin, J. Citrin, L. Garzotti, M. Valovic, C. Bourdelle, Y. Camenen, F. J. Casson, A. Ho, F. Koechl, M. Maslov, JET contributors

Multipe-isotope pellet cycles captured by turbulent transport modelling in the JET tokamak

M. Marin[1], J. Citrin[1], L. Garzotti[2], M. Valovic[2], C. Bourdelle[4], Y. Camenen[3],
F. J. Casson[2], A. Ho[1], F. Koechl[5], M. Maslov[2] and JET contributors[6]

[1] DIFFER - Dutch Institute for Fundamental Energy Research, Eindhoven, The Netherlands
[2] CCFE, Culham Science Centre, Abingdon, Oxon, OX14 3DB, UK
[3] CNRS, Aix-Marseille Univ., PIIM UMR 7345, Marseille, France
[4] CEA, IRFM, F-13108 Saint-Paul-lez-Durance, France
[5] OAW/ATI, Atominstitut, TU Wien, 1020 Vienna, Austria
[6] See the author list of 'Overview of the JET preparation for Deuterium-Tritium Operation' by E. Joffrin
et al 2019 Nucl. Fusion 59 112021 https://iopscience.iop.org/article/10.1088/1741-4326/ab2276

(Dated: May 12, 2020)

The pellet cycle of a mixed isotope tokamak plasma is successfully reproduced with reduced turbulent transport modelling within an integrated simulation framework. In JET tokamak experiments, deuterium pellets with reactor-relevant deposition characteristics were injected into a pure hydrogen plasma. Measurements of the isotope ratio profile inferred a fast deuterium penetration time comparable to the energy confinement time. The modelling recovered the fast deuterium penetration timescale. The results are encouraging with regard to reactor fuelling capability and burn control.

In present tokamaks, particle fuelling is mainly provided by neutral gas puffing from the plasma periphery and from Neutral Beam Injection (NBI). Gas fuelling may be rendered ineffective in future reactors due to increased neutral opacity, while the particle source from the NBI will be relatively small. A viable alternative as a primary fuelling technique is the injection of cryogenic pellets [1], with higher penetration and faster response times. Pellet mass, injection speed and frequency can be jointly adjusted to optimize the particle source and provide fuelling in the plasma core, where the pellet is ablated. In ITER, for example, pellets of mass between 2 and $5.5 \cdot 10^{21}$ atoms with frequency between 1.5 and 3.5 Hz respectively should be sufficient to maintain the density required for a Q=10 baseline ELMy H-mode scenario at 15 MA.

Active research on pellet fuelling focuses on its compatibility with integrated plasma scenario constraints, including control of MagnetoHydroDynamic (MHD) modes such as Edge Localised Modes (ELMs), plasma exhaust, core turbulent transport, and desired isotope composition. Previous integrated tokamak plasma simulation (integrated modelling) including pellets focused on various aspects of the pellet cycle: improved confinement regimes [2, 3, 4], edge and fuelling requirements [5], the impact of fuelling on divertor heat-loads [6, 7] and the extrapolation of pellet penetration and transport [8].

Pellet fuelling and simultaneous ELMs mitigation have been demonstrated experimentally [9, 10, 11], ensuring the viability of this fuelling method. Regarding turbulent transport, the pellets have a significant impact. During the ablation phase of the pellet cycle, the density and temperature profiles are transiently modified, changing the micro-instability properties of the discharge. While the heightened negative radial density gradient that develops in the region outside the pellet ablation region is expected to destabilize Trapped Electron Modes (TEM) and lead to a strong outward particle flux [12], the posi-

tive density gradient that develops at radii within the ablation location may stabilize Ion Temperature Gradient (ITG) driven turbulence and reduce the fuel penetration. This was observed for example in the Mega Amp Spherical Tokamak (MAST) [13]. The stabilization was instead counteracted by a larger R/L_T again in MAST, with different plasma conditions, [14] and in a similar JET experiment [15]. This Letter focuses on pellet fuelling in JET mixed isotope plasmas, in an ITER-relevant pellet deposition regime.

In reactors, pellet injection with varying isotope ratios will be used to maintain the desired concentrations of deuterium and tritium in the core; equal ratios ensures maximal fusion power, and burn control is achieved by modifying the relative isotope concentrations. Understanding the timescales for the transport of different isotopes following modification of the pellet isotope composition is fundamental for understanding and predicting burn control. Since the electron and ion particle fluxes must always be equal (ambipolarity), differences in their transport can only be observed experimentally in presence of multiple ion types, e.g. hydrogenic isotopes. Previous experiments observed a fast mixing of T-trace in the Tokamak Fusion Test Reactor (TFTR) [16] and large He transport in AUG [17]. Theoretical analysis recently explained the fast isotope mixing by $D_i/D_e > 1$ and $|V_i| > |V_e|$ in ITG dominated plasmas [18], where D_s and V_s are the species dependent diffusion and pinch coefficients respectively. In a multi-ion plasma the different ions can interchange at different timescales to the electron particle transport. The opposite relation holds for TEM dominated regimes, as shown experimentally in the Large Helical Device (LHD) [19].

Multiple-isotope experiments at JET allowed a detailed investigation of ion particle transport [20]. The effect of the particle sources (gas-puff and NBI) on the isotope profiles was studied, suggesting fast isotope mixing. These experimental observations were success-

fully reproduced in stationary-state, multiple-isotope integrated modelling [21], applying the quasilinear gyrokinetic transport model QuaLiKiz [22, 23], strengthening QuaLiKiz validation in multiple-isotope regimes.

The fast mixing will be most prevalent during transient states, such as during pellet injections, due to the significant modifications of the local density gradients created by the short ablation time of the pellets. Modifying the pellet isotope ratio compared to the background isotope ratio leads to rapid mixing of ions, significantly modifying the core isotope mix without affecting the time averaged electron profile. An experiment was performed at JET precisely with the aim of using pure deuterium pellets to control the core isotope ratio, starting from a pure hydrogen plasma [24].

Relevant parameters of the discharge under investigation are shown in table I. In this experiment the size of the pellets, scaled to the plasma volume, lead to shallow deposition and transient inverted density profile, similarly to what is expected in ITER.

The experiment managed to reach the desired core isotope composition, measured by Balmer-alpha Charge Exchange (CX) spectroscopy and D-D neutron rate. A rapid increase in the neutron rate following the initial pellet injection was observed, faster than the energy confinement time. This observation indicates fast isotope mixing. The isotope particle transport coefficients were determined by interpretative modelling [9], using the semi-empirical Bohm/Gyrobohm turbulent transport model and matching the transient response of the thermal D-D neutron rates. HPI2 [25] was used as the pellet deposition model, showing good agreement with the experiment. The key observation was that $D_D/\chi_{eff} \sim 1$ was inferred at the beginning of the pellet train, where D_D is the diffusion coefficient for Deuterium and χ_{eff} is the effective heat conductivity. Since $D_e/\chi_{eff} << 1$ is expected in the experiment, this finding implies a large D_D/D_e, indeed consistent with the fast isotope mixing.

This Letter demonstrates, for the first time, that multiple pellet cycles and the associated fast isotope mixing can be captured by turbulent transport models within an integrated modelling framework.

The modelling was performed within the JETTO [26] framework, with NCLASS [27] as the neoclassical transport model and QuaLiKiz as the turbulent transport model. The initial electron density and ion and electron temperature profiles were obtained through Gaussian Process Regression (GPR) [28] on the experimental data, averaged for 200ms immediately before the first pellet. PENCIL [29] and PION [30] were used for NBI and ICRH heating respectively, FRANTIC [31] for the neutral source and HPI2 for the pellet ablation. The magnetic equilibrium was evolved self-consistently using ESCO [32].

EFIT++ was used to obtain the last-closed-flux-surface boundary conditions for ESCO. Standard EFIT [33] reconstruction was used to obtain an initial current profile, which was then evolved with ESCO while main-
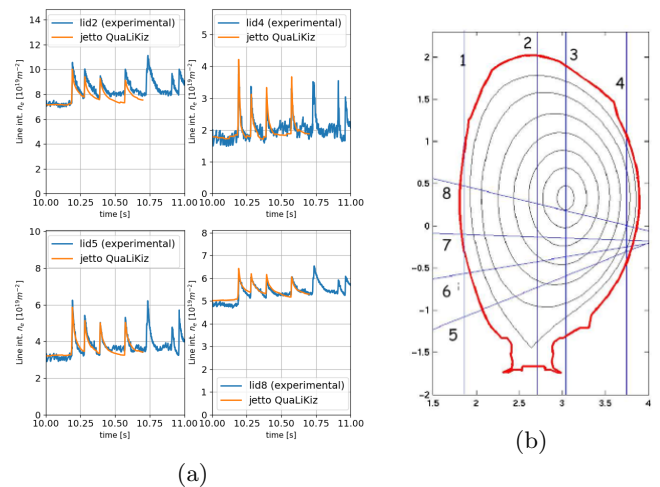
FIG. 1: a) Four different experimental interferometer lines (solid blue lines) for shot #91393, compared with a synthetic diagnostic in JINTRAC (solid orange lines). The pellets are injected at $t = 10.187, 10.278, 10.390, 10.572$. b) Sketch showing the position of the lines of sight of the interferometer at JET

taining the measured kinetic profiles fixed in time. The evolution was stopped when the safety factor $(q) = 1$ surface approached the observed sawteeth inversion radius. This new current profile was used as the initial condition for the pellet-cycle predictive simulations.

Beryllium and Nickel, consistently observed in JET discharges with Ion Cyclotron Resonance Heating (ICRH) [34, 35], were chosen as impurities to match both dilution and Z_{eff}. In NBI heated JET pulses, the centrifugal effects require the 2D neoclassical transport calculations for Tungsten transport [36, 37]. Here, given that the radiated power in the core is below 20% of the heating power, the Tungsten content was inferred to be low and to reduce computational expense was not included the simulation. SANCO [38] was used for the impurity evolution with neoclassical and turbulent transport coefficients calculated again by NCLASS and QuaLiKiz.

Since QuaLiKiz is restricted to electrostatic turbulence, an ad-hoc model was employed to simulate the level of electromagnetic (EM) stabilization, as done previously [37]. Dedicated linear runs with the gyrokinetic code GENE [39] suggested a significant impact of EM-stabilisation on the linear growth rates at inner radii, justifying the inclusion of this effect.

The radial zone incorporating QuaLiKiz-predicted turbulent transport was $0.2 < \rho < 0.94$, with ρ being the normalised toroidal flux coordinate $\rho_{tor} = (\frac{\psi_{tor}}{\psi_{tor,LCFS}})^{\frac{1}{2}}$. For $\rho < 0.2$ modest heat and particle ad-hoc transport was artificially added. This term takes into account the average transport originating from intermittent (1,1) MHD activity (sawteeth). The pedestal region,

TABLE I: Key parameters of JET shot #91393. β here is defined as $2\mu_0 \frac{2}{3} a_{min} * W_{tot}/(I_p * V * B_{geo})$, with $a_{min} = 0.5 * (R_{out,LCFS} - R_{in,LCFS})$, B_{geo} the vacuum toroidal field at the geometric plasma centre and V the volume

I_p [MA]	B [T]	Z_{eff}	P_{NBI} [MW]	P_{ICRH} [MW]	$\Phi_{H2,gas}[10^{21}at/s]$	$f_{pel}[Hz]$	$\Phi_{pel}[10^{21}at/s]$	β	discharge #
1.4	1.7	1.4	8.4	3	6.7	11.4	8.2	1.1 %	91393
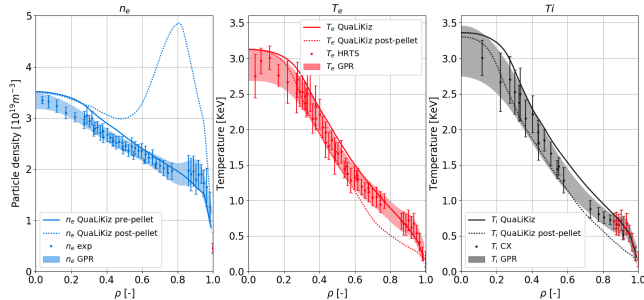
FIG. 2: The shaded area represents the GPR confidence interval, with the experimental data averaged between $9.5s < t < 10.15s$. The solid line is the JETTO-QuaLiKiz prediction for density and temperature profiles before the first pellet ($t = 10.18s$), after ~ 2 particle confinement times of relaxation. The boundary conditions at the Last Close Flux Surface (LCFS) are: $n_{e_1} = 0.7 \cdot 10^{19}[m^{-3}]$, $T_e = T_i = 100[eV]$ The dotted lines show the profiles just after the first pellet injection ($t = 10.19s$)

$0.94 < \rho < 1$, is out of the scope of the QuaLiKiz model, due to the nature of the pedestal turbulence and its suppression, as well as intermittent MHD activity (ELMs).

The typical core transport modeling approach is to take a boundary condition at a radius deeper than the pedestal top, e.g. at $\rho = 0.85$. However, the perturbation caused by the pellet modifies the profiles for $\rho > 0.85$ in a non trivial way. The pedestal was therefore evolved using a "continuous ELM model". The idea here is simply to match the temperature and density evolution at the top of the pedestal and provide appropriate core boundary conditions. The transport in the Edge Transport Barrier (ETB) is treated by the continuous ELM model described in [8], which mimics the limiting effect of the ELMs on the pressure gradient in the ETB by introducing additional transport averaged over time and clamps the normalized pressure gradient in the ETB, α, at a prescribed critical value, α_c, fitted to the experimental value. The parameters in this model were adjusted to match the interferometer measurement of the line of sight looking at the pedestal, indicated with '4' in Figure 1b, with a synthetic diagnostic within JETTO. The result is seen in Figure 1a. This decision resulted in a n_e at the top of the pedestal on the lower end of the error-bar with respect to the GPR fit, as shown in Figure 2, which suffers from lower precision in that region due to the presence of ELMs. These parameters were kept con-

stant during the simulation, meaning that phenomena such as the changes in the ELM behaviour that can be seen in the second panel of Figure 1a after 10.5s are not reproduced. Outward particle convection was added as $v = v_0 \times exp\{-(t-t_{pel})/\tau + (r/a-1)/\Delta\}$ where v_0, τ and Δ are parameters fitted to match the total density. The need for this term, which mimics the extra ELMs density pump out in the presence of pellets, was recognized in previous works [40].

The pellet cycle modelling initial condition corresponded to the stationary state JINTRAC-QuaLiKiz solution of the experimental configuration, after relaxing for ~ 2 particle confinement times, just before the beginning of the pellet train. This is shown in Figure 2.

The good agreement shown in Figure 2 was reached in T_e and T_i, while n_e peaking was slightly overestimated. This general agreement provides confidence that the turbulent regime is correctly captured. The slight trend for improved predicted core confinement for this hydrogen plasma, compared to the measured profiles, may be a result of QuaLiKiz gyroBohm scaling. The nonlinear saturation rule was fit to deuterium plasma gyrokinetic simulations, while observations and nonlinear gyrokinetic simulations show an inverse isotope confinement scaling, with worse confinement for hydrogen [41].

Concerning the dynamic comparison with the experiments, four pellets were modelled, from $t = 10.0s$ to $t = 10.7s$. The model proved robust in responding to the significant changes in the profiles introduced by the pellets. All the measured interferometer lines of sight were compared with a synthetic diagnostic, resulting in general good agreement as shown in Figure 1a. The gradients for two radial points before and after the first pellet are listed in table II and shown in the dotted lines of Figure 2, illustrating the significant modification induced by the transient pellet injection. A direct comparison between the experimental and modelled neutron rate, which is a direct marker of inner-core deuterium content, was carried out.

The $\frac{n_D}{n_e}$ ratio is heavily dependent on the edge transport conditions, which are not predicted in the simulations. The edge transport model free parameters where adjusted to match the final neutron rate to the experimental value. These parameters were the constant recycling coefficient for deuterium in FRANTIC and the minimum deuterium transport coefficient in the ETB model. The deuterium content at the LCFS was increased linearly starting from the first pellet, reaching 20% by the end of the simulation, as measured by Balmer-alpha and Penning gauges. The experimental and modelled neutron
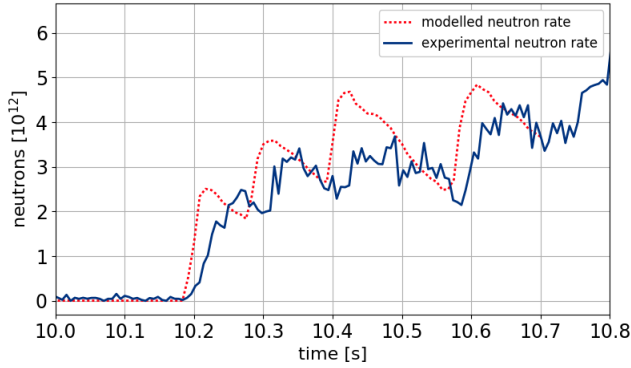
FIG. 3: Measured neutron rate (blue solid line) vs the simulated neutron rate (red dashed line). The fast timescale of D penetration is captured by the modelling
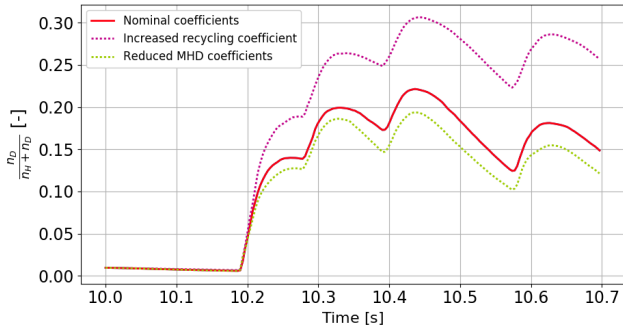
FIG. 4: The red solid line is the n_D/n_e ratio at $\rho = 0.15$ for JET shot #91393 as predicted by JETTO-QuaLiKiz with nominal pedestal coefficients. The green dotted line has increased deuterium recycling coefficient in FRANTIC and the yellow dotted line has reduced scale factors in the continuous ELM model. The fast penetration of D is resilient to the precise tuning of the edge models

rate were found to be in good agreement, as can be seen in Figure 3. All the assumptions made in the integrated modelling can impact both the absolute value and the temporal evolution timescales of the neutron rate. Since the absolute value is ultimately the result of a fit, for each assumption the important sensitivity is on the time

TABLE II: Density and temperature gradients before ($t = 10.185s$) and after ($t = 10.189s$) the first pellet. The two radial positions were chosen to isolate the large positive and negative density gradients induced promptly after a pellet deposition

Gradient	Pre-Pellet			Post-Pellet		
	R/L_{T_i}	R/L_{T_e}	R/L_{n_e}	R/L_{T_i}	R/L_{T_e}	R/L_{n_e}
$\rho = 0.68$	7.4	7.7	2.8	14.4	18.1	-11.4
$\rho = 0.85$	11.1	12.2	5.6	9.5	8.8	14.4
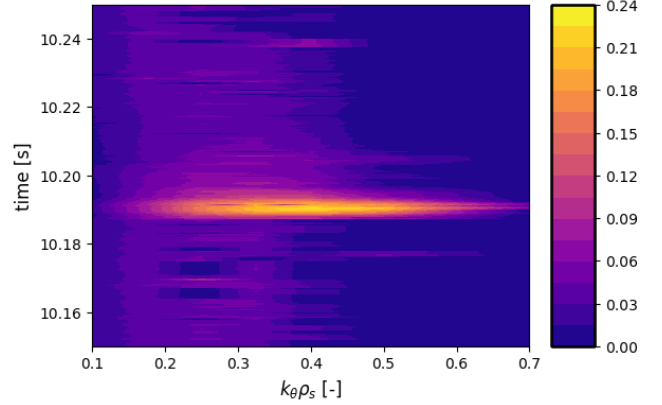
FIG. 5: Growth rates in GyroBohm units for $\rho = 0.64$ during the first pellet cycle. $k_\theta \rho_s$ is the normalized wavenumber $k_\theta \frac{\sqrt{T_e m_i}}{q_e B}$, with m_i being hydrogen mass.

evolution. This is crucial. Extensive tests were carried out, finding in general a small impact on the timescales of the deuterium penetration. The impact of the recycling coefficient and the minimum deuterium transport coefficient are shown in Figure 4.

The deuterium transport timescale was comparable to the energy confinement time. In particular, the rapid evolution of the neutron rate after the first pellet was correctly reproduced in the model. This timescale depends on the turbulent regime and the agreement is a validation of the fast isotope mixing and of both QuaLiKiz and HPI2. The resilience of the fast time scale suggests a high reliability of the isotope penetration predictions in this scenario.

The results are a consequence of the turbulence regime identified by QuaLiKiz. Depending on the radial position and on the phase of the pellet cycle, different modes are excited. TEM was found by QuaLiKiz to be the dominant instability following pellet injection outside $\rho = 0.8$, where most of the pellet is ablated, in conjunction with a very large negative density gradient. This causes a large particle flux directed outwards, in line with expectations from previous works [42]. However, in spite of this strong outward flux, pellet fuelling as observed by the inward deuterium penetration was achieved.

In this case, immediately after the pellet injection, the cooling caused by the adiabatic ablation of the pellets results in a locally steeper R/L_T gradient for $\rho < 0.8$. This balances the stabilizing impact of negative R/L_n which occurs for ITG modes with kinetic electrons. The temporal behaviour of the instabilities, as predicted by QuaLiKiz, with ITG destabilized over a broad spectrum just after the pellet at $t \sim 10.19s$, is illustrated in figure 5. This is key since the fast mixing of the deuterium depends on the ITG drive. To verify this important observation, eigenvalue solutions from QuaLiKiz was compared with linear calculations using the higher fidelity code GENE at $\rho = 0.7$, where R/L_n is large and negative after the

pellet is injected. The growth rate comparison is shown in figure 6 for time slices just before and 10ms after the pellet. The input parameters were taken directly from the integrated modelling simulation.

In the pre-pellet phase, ITG modes dominate for $k_\theta \rho_s < 0.6$. QuaLiKiz predicts lower growth rates than GENE, but with a very similar spectral shape. An increase of the ion temperature gradient by 20% is sufficient for QuaLiKiz to retrieve the GENE growth rates. TEM is found to be unstable by GENE and stable by QuaLiKiz for $k_\theta \rho_s > 0.6$, but is responsible for only a small fraction of the total transport. Additionally, the presence of TEM does not affect the central result of the fast isotope mixing, since in a mixed ITG - TEM regime both ion and electron particle transport are expected to be fast [21]. In the post-pellet phase, ITG again dominates in the transport driving region $k_\theta \rho_s < 0.6$. QuaLiKiz and GENE growth rates agree very well at nominal input parameters in this region. TEM is the dominate mode in GENE for $k_\theta \rho_s > 0.6$. The key result is that indeed ITG is destabilized in GENE in presence of a positive density gradient in the post-pellet phase, validating the QuaLiKiz predictions that resulted in fast isotope mixing.

In future reactors the collisionality will be lower and the heating will be dominated by electron heating from fusion-generated alpha particles. The turbulence regime is predicted to be mixed ITG-TEM [43]. It is therefore important to model such a regime to assess the extrapolability of the fast isotope mixing effect to reactor-relevant plasmas. Some insight was gained here by repeating the same integrated modelling simulations while artificially reducing the collisionality input into QuaLiKiz by a factor 20, towards reactor-relevant values. The turbulent regime is modified to a mixed ITG-TEM regime and the density peaking increases. However, ITG is still destabilised by the pellet at low wavenumbers and significantly contributes to the ion heat and particle transport. The timescale for the deuterium penetration is almost unchanged, confirming that it only depends on ITG being sufficiently destabilized and not on it being the sole dominant instability.

A. Conclusions

The JETTO integrated modelling framework with the turbulent transport model QuaLiKiz as the turbulent transport model and HPI2 as the pellet deposition model successfully reproduced observations over multiple pellet cycles in JET mixed-isotope experiments. Good agreement on the density profile evolution and on the neutron rate timescales was achieved. The compensation between R/L_n stabilization and R/L_T destabilization was shown to lead to maintained ITG drive and allow prompt isotope mixing on energy confinement timescales following each pellet injection throughout the pellet train. The key QuaLiKiz prediction of ITG instability in post-pellet

(a)

(b)
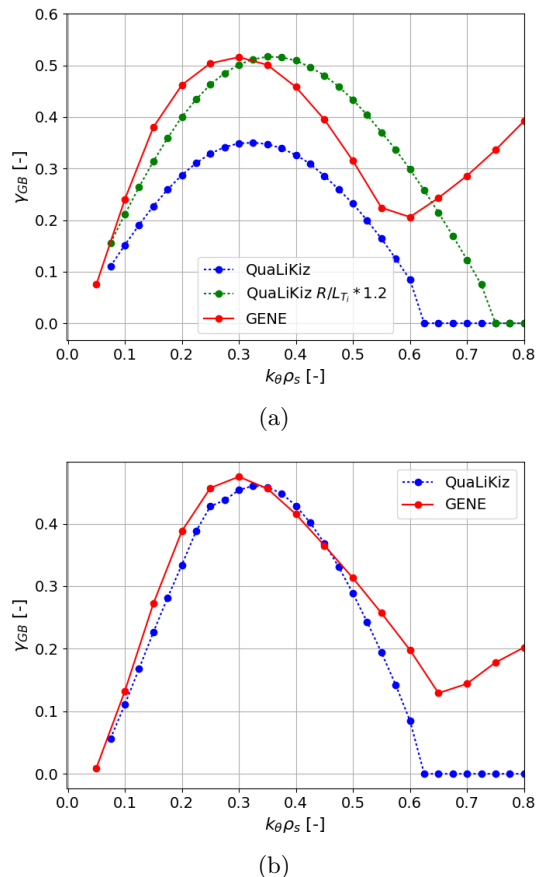
FIG. 6: Comparison between the normalized growth rates from GENE (red solid line) and QuaLiKiz (green and blue dotted lines). The parameters for both scans are taken from the JETTO simulation at $\rho = 0.7$ just before 6a and 10ms after (b) the first pellet. In the upper panel, the green points indicate a simulation where R/L_{T_i} was increased by 20%, while the green points indicate a simulation with nominal R/L_{T_i}. In GENE, the mode switches from the ion to the electron diamagnetic direction for $k_\theta \rho_s > 0.6$ in the upper panel (a) and for $k_\theta \rho_s > 0.5$ in the lower panel (b). 's' indicates the main species, hydrogen in this case. The modes for QuaLiKiz are in the ion diamagnetic direction over the whole spectrum.

negative R/L_n regimes was verified by linear-GENE simulations. The same approach presented in this Letter can be used to predict the pellet cycle in ITER and future reactors, with optimistic preliminary results with regard to fuelling capability and burn control.

Commission.

REFERENCES

[1] E. J. Doyle et al. "Chapter 2: Plasma confinement and transport". In: *Nuclear Fusion* (2007). ISSN: 00295515. DOI: 10.1088/0029-5515/47/6/S02.

[2] D. Frigione et al. "Pellet injection and high density ITB formation in JET advanced tokamak plasmas". In: *Nuclear Fusion* 47.2 (2007), pp. 74–84. ISSN: 00295515. DOI: 10.1088/0029-5515/47/2/002.

[3] L. Garzotti et al. "Simulations of JET pellet fuelled ITB plasmas". In: *Nuclear Fusion* 46.1 (2006), pp. 73–81. ISSN: 00295515. DOI: 10.1088/0029-5515/46/1/009.

[4] M. Romanelli, C. Bourdelle, and W. Dorland. "Effects of high density peaking and high collisionality on the stabilization of the electrostatic turbulence in the Frascati Tokamak Upgrade". In: *Physics of Plasmas* 11.8 (2004), pp. 3845–3853. ISSN: 1070664X. DOI: 10.1063/1.1766031.

[5] A. R. Polevoi et al. "Integrated simulations of H-mode operation in ITER including core fuelling, divertor detachment and ELM control". In: *Nuclear Fusion* 58.5 (2018). ISSN: 17414326. DOI: 10.1088/1741-4326/aab4ad.

[6] S. Wiesen et al. "Control of particle and power exhaust in pellet fuelled ITER DT scenarios employing integrated models". In: *Nuclear Fusion* 57.7 (2017). ISSN: 17414326. DOI: 10.1088/1741-4326/aa6ecc.

[7] L. Garzotti et al. "Integrated core-SOL modelling of fuelling, density control and divertor heat loads for the flat-top phase of the ITER H-mode D-T plasma scenarios". In: *Nuclear Fusion* 59.2 (2019), p. 026006. ISSN: 17414326. DOI: 10.1088/1741-4326/aaf2f3.

[8] V. Parail et al. "Integrated modelling of ITER reference scenarios". In: *Nuclear Fusion* 49.7 (2009). ISSN: 00295515. DOI: 10.1088/0029-5515/49/7/075030.

[9] M. Valovic et al. "Density control by pellets in plasmas with ELM mitigation by RMPs in the ASDEX Upgrade tokamak". In: *Plasma Physics and Controlled Fusion* 60.8 (2018).

[10] M Valovic et al. "Compatibility of pellet fuelling with ELM suppression by RMPs in the ASDEX Upgrade tokamak". In: *Nucl. Fusion* 60 (2020), p. 054006.

[11] P. T. Lang et al. "High-density H-mode operation by pellet injection and ELM mitigation with the new active in-vessel saddle coils in ASDEX Upgrade". In: *Nuclear Fusion* 52.2 (2012), p. 023017. ISSN: 00295515. DOI: 10.1088/0029-5515/52/2/023017.

[12] L. Garzotti et al. "Particle transport and density profile analysis of different JET plasmas". In: *Nuclear Fusion* 43.12 (2003), pp. 1829–1836. ISSN: 00295515. DOI: 10.1088/0029-5515/43/12/025.

[13] L. Garzotti et al. "Microstability analysis of pellet fuelled discharges in MAST". In: *Plasma Physics and Controlled Fusion* 56.3 (2014), p. 035004. ISSN: 07413335. DOI: 10.1088/0741-3335/56/3/035004.

[14] M. Valovic et al. "Particle confinement of pellet-fuelled tokamak plasma". In: *Nucl* 48.7 (2008), p. 075006.

[15] D. Tegnered et al. "Gyrokinetic simulations of particle transport in pellet fuelled JET discharges". In: *Plasma Physics and Controlled Fusion* 59.10 (2017). ISSN: 13616587. DOI: 10.1088/1361-6587/aa7a84.

[16] P. C. Efthimion et al. "Tritium particle transport experiments on TFTR during D-T operation". In: *Physical Review Letters* (1995). ISSN: 00319007. DOI: 10.1103/PhysRevLett.75.85.

[17] C. Angioni et al. "Gyrokinetic simulations of impurity, He ash and α particle transport and consequences on ITER transport modelling". In: *Nuclear Fusion* (2009). ISSN: 00295515. DOI: 10.1088/0029-5515/49/5/055013.

[18] C. Bourdelle et al. "Fast H isotope and impurity mixing in ion-temperature-gradient turbulence". In: *Nuclear Fusion* 58.7 (2018), p. 076028. ISSN: 0029-5515. DOI: 10.1088/1741-4326/aacd57.

[19] K Ida et al. "Transition between Isotope-Mixing and Nonmixing States in Hydrogen-Deuterium Mixture Plasmas". In: *Physical Review Letters* 124.2 (2020), p. 25002. ISSN: 1079-7114. DOI: 10.1103/PhysRevLett.124.025002. URL: https://doi.org/10.1103/PhysRevLett.124.025002.

[20] M. Maslov et al. "Observation of enhanced ion particle transport in mixed H/D isotope plasmas on JET". In: *Nuclear Fusion* 58 (2018), p. 076022. ISSN: 17414326. DOI: 10.1088/1741-4326/aac342.

[21] M. Marin et al. "First-principles-based multiple-isotope particle transport modelling at JET". In: *Nuclear Fusion* 60.4 (2020), p. 046007. ISSN: 0029-5515. DOI: 10.1088/1741-4326/ab60d1.

[22] C. Bourdelle et al. "Core turbulent transport in tokamak plasmas: Bridging theory and experiment with QuaLiKiz". In: *Plasma Physics and Controlled Fusion* 58.1 (2016), p. 14036. ISSN: 13616587. DOI: 10.1088/0741-3335/58/1/014036. URL: http://dx.doi.org/10.1088/0741-3335/58/1/014036.

[23] J. Citrin et al. "Tractable flux-driven temperature, density, and rotation profile evolution with the quasilinear gyrokinetic transport model QuaLiKiz". In: *Plasma Physics and Controlled Fusion* 59.12 (2017), p. 124005. ISSN: 13616587. DOI: 10.1088/1361-6587/aa8aeb. arXiv: 1708.01224.

[24] M. Valovič et al. "Control of the hydrogen:deuterium isotope mixture using pellets in JET". In: *Nuclear Fusion* 59.10 (2019), p. 106047. ISSN: 0029-5515. DOI: 10.1088/1741-4326/ab3812. URL: https://doi.org/10.1088/1741-4326/ab3812.

[25] Florian Köchl et al. "Modelling of Pellet Particle Ablation and Deposition : The Hydrogen Pellet Injection code HPI2". In: *Preprint EFDAJETPR(12)57* 12 (2012), p. 82.

[26] Michele Romanelli et al. "JINTRAC: A system of codes for integrated simulation of Tokamak scenarios". In: *Plasma and Fusion Research* 9 (2014). ISSN: 18806821. DOI: 10.1585/pfr.9.3403023.

[27] W. A. Houlberg et al. "Bootstrap current and neoclassical transport in tokamaks of arbitrary collisionality and aspect ratio". In: *Physics of Plasmas* 4 (1997), p. 3230. ISSN: 1070664X. DOI: 10.1063/1.872465.

[28] A. Ho et al. "Application of Gaussian process regression to plasma turbulent transport model validation via integrated modelling". In: *Nuclear Fusion* 59.5 (2019), p. 056007. ISSN: 0029-5515. DOI: 10.1088/1741-4326/ab065a.

[29] C. D. Challis et al. "Non-inductively driven currents in JET". In: *Nuclear Fusion* 29.4 (1989), pp. 563–570. ISSN: 17414326. DOI: 10.1088/0029-5515/29/4/002.

[30] L. G. Eriksson, T. Hellsten, and U. Willen. "Comparison of time dependent simulations with experiments in ion cyclotron heated plasmas". In: *Nuclear Fusion* 33.7 (1993), pp. 1037–1048. ISSN: 00295515. DOI: 10.1088/0029-5515/33/7/I07.

[31] S Tamor. "ANTIC: A code for Calculation of Neutral Transport in Cylindrical Plasmas". In: *Journal of Computational Physics* 40.1 (1981), p. 104119. DOI: 10.1016/0021-9991(81)90202-3.

[32] G. Cenacchi; M. Romanelli. *JETTO manual*. 2. 1988.

[33] L. L. Lao. "Reconstruction of current profile parameters and plasma shapes in tokamaks". In: *Nuclear Fusion* 25 (1985), p. 1611.

[34] A. Czarnecka et al. "Determination of metal impurity density, Δzeff and dilution on JET by VUV emission spectroscopy". In: *Plasma Physics and Controlled Fusion* 53.3 (2011), pp. 0–16. ISSN: 07413335. DOI: 10.1088/0741-3335/53/3/035009.

[35] M. Sertoli et al. "Measuring the plasma composition in tokamaks with metallic plasma-facing components". In: *Journal of Plasma Physics* 85.5 (2019), pp. 22–27. ISSN: 0022-3778. DOI: 10.1017/s0022377819000618.

[36] S. Breton et al. "First principle integrated modeling of multi-channel transport including Tungsten in JET". In: *Nuclear Fusion* 58 (2018), p. 096003.

[37] F. J. Casson. "" In: *Accepted by Nuclear Fusion* (2020).

[38] B Alper et al. "Impurity Transport of High Performance Discharges in JET". In: *21st EPS 1.102*. 1994, pp. 3–7.

[39] F. Jenko, W. Dorland, M. Kotschenreuther and B. N. Rogers. "Electron Temperature Gradient Driven Turbulence". In: *Turbulent Transport in Magnetized Plasmas* 1904.February 2000 (2000), pp. 338–375. DOI: 10.1142/9789814383547_0014.

[40] F Koechl et al. "Optimising the ITER 15MA DT baseline scenario by exploiting self-consistent-consistent free-boundary core-edge-sol workflow in IMAS". In: *IAEA-EX*. 2018, P7–25.

[41] C. F. Maggi et al. "Isotope effects on L-H threshold and confinement in tokamak plasmas". In: *Plasma Physics and Controlled Fusion* 60.1 (2018), p. 014045. ISSN: 13616587. DOI: 10.1088/1361-6587/aa9901.

[42] C. Angioni, P. T. Lang, and P. Manas. "Density gradient driven microinstabilities and turbulence in ASDEX Upgrade pellet fuelled plasmas". In: *Nuclear Fusion* 57.11 (2017), p. 116053. ISSN: 17414326. DOI: 10.1088/1741-4326/aa8006.

[43] E. Fable et al. "The role of the source versus the collisionality in predicting a reactor density profile as observed on ASDEX Upgrade discharges". In: *Nuclear Fusion* 59.7 (2019), p. 076042. ISSN: 0029-5515. DOI: 10.1088/1741-4326/ab1f28.